Catalysis
Science &
Technology

rsc.li/catalysis

Volume 7
Number 2
21 January 2017
Pages 313–534

ISSN 2044-4761

ROYAL SOCIETY OF CHEMISTRY

PAPER
Chaoqiu Chen, Yong Qin et al.
Highly dispersed Pt nanoparticles supported on carbon
nanotubes produced by atomic layer deposition for hydrogen
generation from hydrolysis of ammonia borane

ROYAL SOCIETY OF CHEMISTRY

rsc.li/catalysis

ARTICLE

Photocatalytic decarboxylative deuteration of lauric acid with heavy water for sustainable synthesis of deuterated alkanes

Haifan Huang,[a] Zihan Lin,[a] Akira Yamamoto,[a] Bhoi Yagna Prakash,[a] Kexin Zou,[a] Shohichi Furukawa,[a] Ken-ichi Fujita,[a] Gunik Lee,[b] Jun Kumagai[c] and Hisao Yoshida*[a]

As a simple model system for sustainable synthesis of deuterated alkanes, photocatalytic decarboxylative deuteration of lauric acid (dodecanoic acid) was explored employing heavy water (^2H_2O, D_2O) as the deuterium source and titanium dioxide (TiO_2) photocatalysts loaded with metal cocatalysts (Au, Pt or Pd), without requiring any reducing reagents. The photocatalysts effectively facilitated the production of monodeuterated undecane ([$^2H_1$]undecane, $C_{11}H_{23}D$). The alkyl radical degenerated from lauric acid through decarboxylation couples with deuterium radical generated from heavy water, resulting in the formation of the deuterated undecane. Among the tested photocatalysts, a gold-loaded TiO_2 (Au/TiO_2) photocatalyst pre-dried before use achieved a 15.3 % yield of deuterated undecane after 3 hours of photocatalytic reaction, with the deuteration ratio (R_d) in obtained undecane reaching 85.1 %. While extending the reaction time increased the overall yield, it led to a lower R_d. The R_d did not reach 100 % since the alkyl radical intermediate also reacts with lauric acid or forms hydrocarbons to form non-deuterated undecane ($C_{11}H_{24}$) as a byproduct. The reaction mechanism of this photocatalytic system was elucidated using ESR measurement with radical trapping. This study offers a model methodology for efficient synthesis of deuterated compounds, with potential applications in various fields such as pharmaceuticals.

Introduction

Since the discovery of deuterium (^2H, or D), an isotope of hydrogen, in 1931,[1] deuterated compounds have played a crucial role in elucidating chemical reaction processes and mechanisms.[2,3] Deuterium is a cost-effective, safer, and more accessible labeling alternative compared to other isotopes[4] such as ^{13}C, ^{14}C, and ^3H. Additionally, the slower dissociation rate of the bond between deuterium and carbon provides distinct properties when compared to the typical hydrogen isotope (^1H). Recently, deuterium-labeled drugs have shown significant potential in drug development, as they are expected to extend the half-life of drug metabolism due to their slow reaction rate. For example, the first deuterated drug, Austedo (deuterated tetrabenazine), was approved by the US FDA in 2017 for the treatment of movement disorders.[5,6] Austedo is a modified form of tetrabenazine incorporating two deuterated methyl groups (including six deuterium atoms), which results in a drug with a prolonged life-time. Given these advancements, developing effective deuteration methods is of great significance in both pharmaceutical research and production. In the past few years, considerable attention has been devoted to the development of new methods for the deuteration of organic molecules. Emerging techniques include reductive and deuterodehalogenation, photoredox-catalyzed labeling, and the development of transition metals systems.[7] Recently, some outstanding deuteration reactions have also been summarized in some review articles.[8–12]

Several primary methods for incorporating deuterium into an organic molecule include conventional multistep synthesis and direct hydrogen isotope exchange (HIE).[4,13,14] For instance, Kerr, et al.,[15] used D_2 as a deuterium source with homogeneous iridium catalysts to selectively deuterate indole, azaindole, and pyrrole N-heterocycles. Traditional HIEs processes often require harsh conditions such as strong acids/bases,[16–20] flammable gases,[21–23] multiple exchange processes[24–27] to ensure efficient deuterium incorporation. In addition, some cases involve costly deuterium sources.[28,29] Meanwhile, the precise and selective introduction of deuterium typically relies on functional groups like halogens, which can offer better position selectivity and efficiency than C–H/C–D exchange reactions. However, this approach still requires complex ligands and special deuterium donors like Et_3SiD[30] or Ph_2CDOH.[31] Furthermore, the large-scale applications of halogen-based methods raise environmental concerns. Therefore, there is a growing need for new, cost-effective, and environmentally friendly deuteration methodologies.

Photocatalytic synthesis has emerged as a promising approach for selective introduction of deuterium on organic molecules under mild conditions. Recent studies have reported photocatalytic dehalogenative deuteration of aryl halides using D_2O or CD_3CN as deuterium sources with photocatalysts such as Au/Cds,[13] CdSe,[32] and MOF.[33] However, these methods require the use of reducing reagents. Titanium oxide (TiO_2) photocatalyst, as a well-known semiconductor photocatalyst, can play a crucial role in the decomposition of organic

a. Graduate School of Human and Environmental Studies, Kyoto University, Yoshida-nihonmatsu-cho, Sakyo-ku, Kyoto 606-8501, Japan.
b. Department of Material Chemistry, Graduate School of Engineering, Nagoya University, Chikusa, Nagoya 464-8603, Japan.
c. Institute of Materials and Systems for Sustainability Division of Materials Research, Nagoya University, Furo-cho, Chikusa-ku, Nagoya, Aichi 464-8601, Japan.
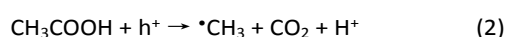† Footnotes relating to the title and/or authors should appear here.
Supplementary Information available: [details of any supplementary information available should be included here]. See DOI: 10.1039/x0xx00000x

pollutants, [34–38] water splitting, [39–44] and carbon dioxide reduction. [45,46] TiO_2 has also demonstrated promising photocatalytic performance in organic synthesis. [47–51] Kraeutler and Bard reported in 1978 that TiO_2 and platinated TiO_2 photocatalysts can produce methane (CH_4) and carbon dioxide (CO_2) primarily from acetic acid (CH_3COOH) aqueous solutions, [52,53] which is known as photo-Kolbe reaction (Eq. 1).

$$CH_3COOH \rightarrow CH_4 + CO_2 \qquad (1)$$
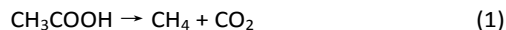
In this reaction, the photocatalyst facilitates both the oxidation of acetic acid by holes to form methyl radicals ($^\bullet CH_3$), CO_2, and protons (Eq. 2) as well as the reduction of protons by electrons to form hydrogen radicals ($H^\bullet$, Eq. 3). These radicals then couple to produce CH_4 (Eq. 4). Potential byproducts of this reaction include hydrogen and ethane, which are formed via radical homocoupling (Eq. 5 and 6).

$$CH_3COOH + h^+ \rightarrow {}^\bullet CH_3 + CO_2 + H^+ \qquad (2)$$

$$H^+ + e^- \rightarrow H^\bullet \qquad (3)$$

$${}^\bullet CH_3 + H^\bullet \rightarrow CH_4 \qquad (4)$$

$$2H^\bullet \rightarrow H_2 \qquad (5)$$

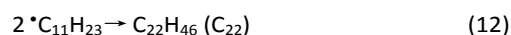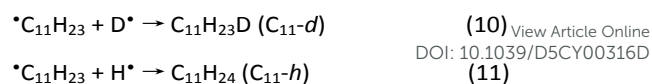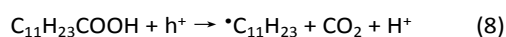$$2 {}^\bullet CH_3 \rightarrow C_2H_6 \qquad (6)$$

Building on this reaction, our laboratory demonstrated a photocatalytic direct methylation of benzene under light irradiation using a platinum-loaded TiO_2 photocatalyst (Pt/TiO_2) with acetic acid as a methylation reagent. [54] This study suggests that the carboxyl group in organic acid (R–COOH) can serve as a possible leaving group, enabling the generation of corresponding alkyl radicals for the chemical reaction during photocatalytic decarboxylation. Organic acids, which commonly contain carboxyl groups, thus provide additional opportunities for deuterated substrates. In recent years, several studies have explored photocatalytic decarboxylative deuteration. [55,56] For example, Li et al [57] achieved precise deuteration of aliphatic carboxylic acids by synergistic photoredox and HAT catalysis, obtaining good deuterium incorporation at predicted sites.

In this study, we explored a simple and sustainable reaction model system for photocatalytic decarboxylative deuteration, using lauric acid (LA) as the substrate and D_2O as the deuterium source to produce deuterated alkanes (Eq. 7). The reaction was conducted with a metal-loaded TiO_2 photocatalyst under light irradiation, without requiring any reducing reagents.

$$C_{11}H_{23}COOH + D_2O \rightarrow C_{11}H_{23}D + HDO + CO_2 \quad (7)$$
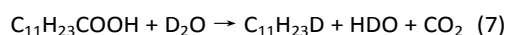
The successful production of the deuterated product was confirmed. In this reaction, alkyl radicals such as undecyl radical ($^\bullet C_{11}H_{23}$) and deuterium radical ($D^\bullet$) are formed from LA and heavy water prior to the formation of the deuterated undecane ($C_{11}H_{23}D$), denoted as C_{11}-d in the present study (Eq. 8–10) although non-deuterated undecane ($C_{11}H_{24}$, denoted as C_{11}-h) and docosane ($C_{22}H_{46}$, denoted as C_{22}) were also formed as dominant byproducts (Eq. 11, 12)

$$C_{11}H_{23}COOH + h^+ \rightarrow {}^\bullet C_{11}H_{23} + CO_2 + H^+ \qquad (8)$$

$$D^+ + e^- \rightarrow D^\bullet \qquad (9)$$

$${}^\bullet C_{11}H_{23} + D^\bullet \rightarrow C_{11}H_{23}D \ (C_{11}\text{-}d) \qquad (10)$$

$${}^\bullet C_{11}H_{23} + H^\bullet \rightarrow C_{11}H_{24} \ (C_{11}\text{-}h) \qquad (11)$$

$$2 {}^\bullet C_{11}H_{23} \rightarrow C_{22}H_{46} \ (C_{22}) \qquad (12)$$

ESR spectroscopy provided insights into the possible reaction mechanism of this photocatalytic system. These findings demonstrate a straightforward, green, and cost-effective strategy for synthesizing deuterated compounds using organic acid and heavy water, including potential applications in the production of deuterated pharmaceuticals.

Results

Photocatalytic reaction tests with M/TiO_2 photocatalysts

The results of the photocatalytic reaction tests are summarized in Fig. 1A and Table S1. After photoirradiation (wavelength > 360 nm) for 30 min, the target product, deuterated undecane (C_{11}-d), was obtained when TiO_2 or metal-loaded TiO_2 photocatalysts were used. The quantity of C_{11}-d contains one-deuterium undecane (C_{11}-d_1) and little doubly deuterate undecane (C_{11}-d_2, see Fig. S3). In addition, non-deuterated undecane (C_{11}-h) and docosane (C_{22}) were detected as the dominant byproducts. Isomers of C_{22} were observed, though the amounts were very tiny. Further details can be found in the Supplementary information. Under certain conditions, oily products, likely resulting from successive polymerization, were observed. Regarding the gas-phase products, CO_2 and H_2 were detected; however, accurate quantitative analysis remained technically challenging.

Compared with the bare TiO_2 photocatalyst, the Au, Pt, and Pd metal-loaded TiO_2 samples exhibited higher photocatalytic activity for decarboxylation of LA as expected (Fig. 1A). Among the M(0.1)/TiO_2 photocatalysts, the Au(0.1)/TiO_2 sample gave lower total yield (Y_x) and C_{11}-d yield ($Y_{C11\text{-}d}$) but higher selectivity toward C_{11}-d (S_d) compared to the Pt(0.1)/TiO_2 and Pd(0.1)/TiO_2 samples (Table S1). The Pt(0.1)/TiO_2 sample showed the highest overall photocatalytic activity (Y_{total}) but the lowest selectivity to C_{11}-d, suggesting that the higher photocatalytic activity may lead to an increased concentration of alkyl radicals, promoting the formation of C_{22}, thus decreasing S_d value. This sample was employed for the mechanistic study as mentioned later. The Pd(0.1)/TiO_2 sample achieved the highest $Y_{C11\text{-}d}$ (6.68%), though it exhibited a close value of S_d compared to Au(0.1)/TiO_2 sample due to the formation of a significant amount of by-products, C_{11}-h and C_{22}.

The selectivity of deuterated n-undecane (R_d), defined as the ratio of C_{11}-d to the total n-undecane (C_{11}-d and C_{11}-h) obtained, is a key parameter, as the separation of C_{11}-d from the mixture of undecane is very challenging. As shown in Fig. 1A, the Au(0.1)/TiO_2 sample exhibited the highest R_d. In contrast, the Pt(0.1)/TiO_2 and Pd(0.1)/TiO_2 samples showed comparatively lower R_d values. As discussed later, since R_d is determined by the reaction selectivity of the generated alkyl radical toward deuterium radical ($D^\bullet$) or other organic species, the highest R_d value is attributed to the properties of the Au cocatalyst. The

reasons why the highest R_d did not reach 100% with any of the photocatalysts will be discussed later.

Results from blank reaction tests with the Au(0.5)/TiO$_2$ sample (Table S2) indicated that both photoirradiation and the presence of a photocatalyst were essential for the reactions to
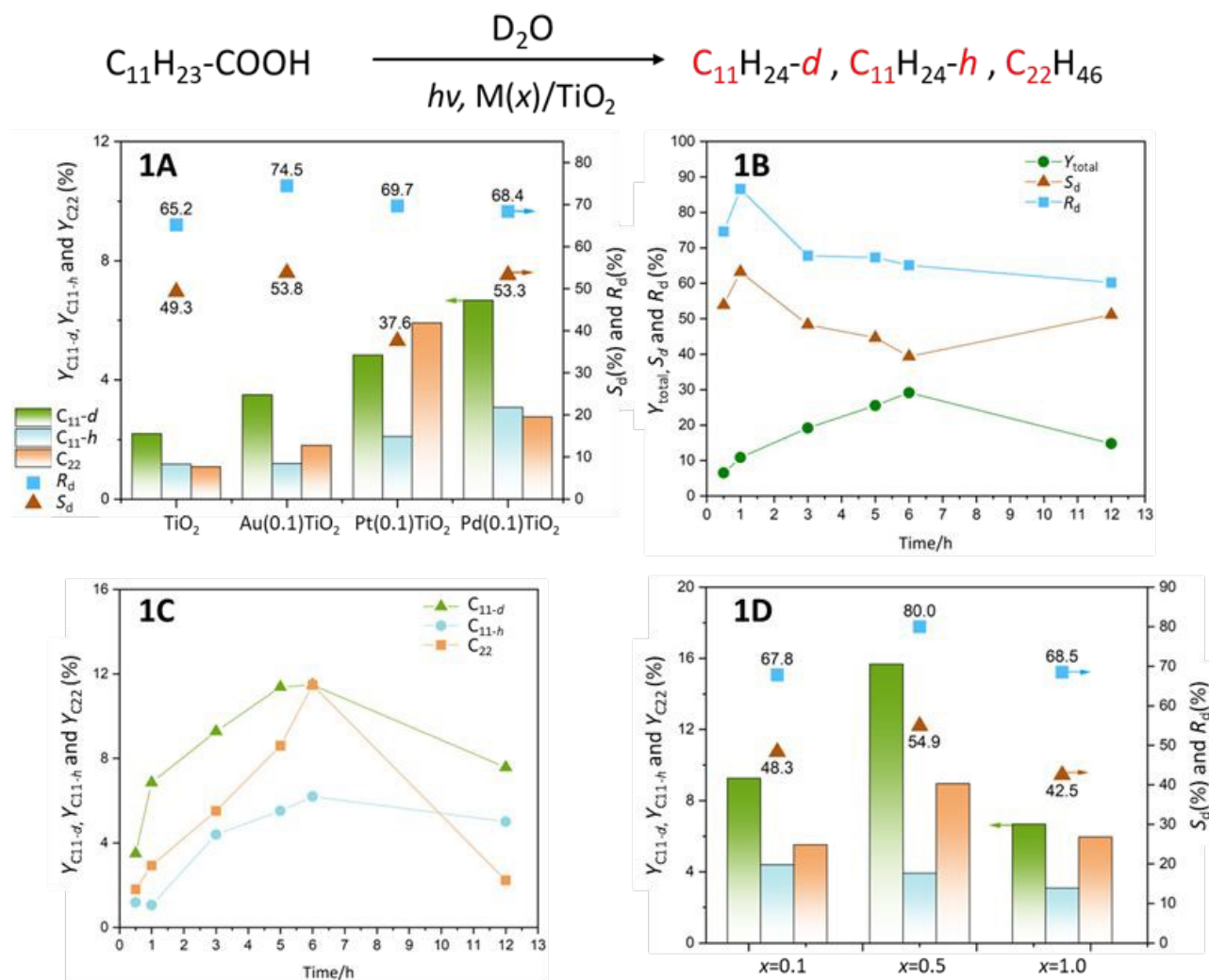

Fig. 1 Results of the reaction tests for photocatalytic decarboxylation of LA in the presence of heavy water: (A) Results with the TiO$_2$ and M(0.1)/TiO$_2$ samples (M=Au, Pt, and Pd). The green, light blue, and orange bars represent. Y_{C11-d}, Y_{C11-h}, and Y_{C22}, respectively. Dark red triangles indicate S_d (selectivity to C$_{11}$-d), and light blue squares show R_d (selectivity to C$_{11}$-d in the obtained undecanes). The reaction time was 0.5 h. Data are taken from Table S1; see the caption of Table S1 for other reaction conditions. (B) Time course of Y_{total}, S_d, and R_d with the Au(0.1)/TiO$_2$ sample. (C) Time courses of Y_{C11-d}, Y_{C11-h}, and Y_{C22} with the Au(0.1)/TiO$_2$ catalysts. Detailed conditions for panels B and C are shown in Table S3. (D) Results of the photocatalytic reaction tests with Au(x)/TiO$_2$ samples with different Au loading amounts (x wt%). The reaction time was 3 h. See also Table S4.

occur, confirming that the deuteration proceeds photocatalytically. The time course study showed that the total yield of the products monotonously increased with time while the S_d and R_d decreased with time (Fig. 1B, Table S3). The product distribution slightly varied with time (Fig. 1C, Table S3). The Y_{C11-h} and Y_{C22} continuously increased, whereas the increase in the Y_{C11-d} slowed down with time. A possible explanation for this variation with time could be the change in the hydrophilic property of the photocatalyst surface due to the adsorption of hydrophobic products. Notably, the amount of main products decreased after 12 h of reaction, indicating

that some successive reactions may happen to convert C$_{11}$-d into other products. Based on these results, the reaction time was set to 3 hours for all subsequent reaction tests. A recyclability test was also carried out, which led to a slight decrease in the C$_{11}$-d yield and R_d value. Details are described in the SI, Fig. S4. To improve the durability of the catalysts, improvements are required in the process of the catalyst recycling, catalyst surface modification, and the improving the property of the loaded co-catalyst metals. By using a flow reactor, it might be possible to avoid these problems. [58]

Since the Au(0.1)/TiO$_2$ sample showed the best R_d value among the three M(0.1)/TiO$_2$ samples (Fig. 1A), additional Au(x)/TiO$_2$ samples were tested with varying Au loading, and the results were presented in Fig. 1D and Table S4. The Au(0.5)/TiO$_2$ sample demonstrated the best performance, achieving a high Y_{C11-d} (15.7%) and a high R_d (80%) in the conditions. It is observed that Au(1.0)/TiO$_2$ exhibited lower activity compared to Au(0.5)/TiO$_2$, as shown in Fig. 1D and Table S4. This decline in performance at higher loadings may be attributed to the aggregation of Au nanoparticles (NPs), which is known to occur when the metal content exceeds a certain threshold. At higher metal loadings, the particle size of metal NPs tends to increase, leading to a reduced surface area. This decrease in surface area may, in turn, lower the efficiency of electron transfer required for the reduction of D$^+$, thus decreasing the overall photocatalytic activity. This phenomenon has been reported in similar systems and highlights the importance of optimizing metal dispersion for maintaining catalytic efficiency. [59–61]

Mechanistic studies

As mentioned above, the R_d could not reach 100% with any of the photocatalysts under these conditions. This suggests that hydrogen (^{1}H) from other compounds or materials reacted with the photocatalytically generated undecyl radical (Eq. 11). To increase the R_d and to elucidate the reaction mechanism, additional experiments were conducted as described below.

Reaction conditions. First, three different ratios of D$_2$O and CH$_3$CN (D$_2$O:CH$_3$CN= 2:3, 1:1, 3:2. v/v) were examined (Fig. 2A). To maintain a constant total reactant volume of 5 mL, 2 mL, 2.5 mL, and 3 mL of D$_2$O were used, corresponding to 40, 50, 60 % of total. Higher D$_2$O proportions resulted in better Y_{C11-d} and higher R_d values. However, since LA does not fully dissolve in solutions with higher concentrations of D$_2$O, experiments using more than 3 mL of D$_2$O were not conducted in the present study. From these results, a high concentration of D$_2$O is beneficial for producing deuterated compounds.

Subsequently, the photocatalytic reaction was carried out at varying light intensities (Fig. 2B). The Y_{C11-d} increased with light intensity, while Y_{C11-h} initially increased until intensity reached 21 mW cm^{-2}, after which it decreased at a higher light intensity. In contrast, Y_{C22} remained relatively stable across different light intensities. These results suggest that the production of C$_{11}$-d is enhanced by light intensity, while the radical coupling process that produces C$_{22}$ is not significantly influenced by light intensity. At higher light intensities, more alkyl radicals are utilized to form C$_{11}$-d rather than C$_{11}$-h. In addition, R_d increased as the light intensity was increased, and further discussion of this trend can be found in the succeeding section.

Pretreatment. To determine whether initial impurities such as adsorbed organic matter, water (^{1}H$_2$O), or hydroxy groups on the surface of the photocatalyst sample could serve as hydrogen (^{1}H) sources or not, we examined alternative pre-treatments. These included pre-heating and pre-irradiation, replacing the typical pre-treatment prior to photocatalytic
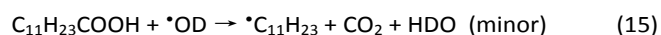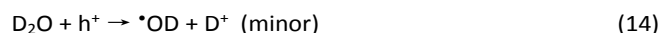
reaction tests. Pre-heating was intended to remove adsorbed organic matter and water, while pre-irradiation was aimed at facilitating H/D exchange of surface hydroxy groups on the photocatalyst before the photocatalytic reaction test.

The results are shown in Fig. 2C and Table S7. Although pre-irradiation without pre-heating enhanced the photocatalytic activity and selectivity for deuterated undecane (S_d), it did not improve R_d (Fig. 2Cb)). In contrast, pre-heating led to higher Y_{C11-d} and an improved R_d, with values of 15.3% and 85.1%, respectively (Fig. 2Cb and 2Cc). Heating the sample in an argon flow at 450 K effectively should remove adsorbed organic matter and water, reducing the formation of C$_{11}$-h and enhancing R_d. Furthermore, when pre-heating was performed, pre-irradiation (with or without D$_2$O) did not significantly impact R_d (Fig. 2Cc and 2Cd). The best result with the highest R_d (85.1%) among them was achieved under the conditions shown in Fig. 2Cc. These findings highlight that removing initially adsorbed impurities on the photocatalyst surface improves R_d, although complete R_d remains still unachieved.

Deuterium sources. Next, we tested the photoreaction using deuterated acetonitrile (CD$_3$CN) instead of CH$_3$CN since the solvent was also a candidate of the hydrogen source. Fig. 2D depicts a set of control experiments conducted in different solvents (CH$_3$CN and CD$_3$CN) and water (D$_2$O and H$_2$O) using the Au(0.5)/TiO$_2$ photocatalyst (See also Table S8). The Y_{C11-d} was not improved by using CD$_3$CN as a solvent (Fig. 2Db), which confirmed that the solvent in this protocol is irrelevant to the synthesis of deuterated alkane. At the same time, it was proved that D$_2$O serves as the only deuterium source in this system, which is the same as the results in literature: For instance, in the case of the CdSe photocatalyst used for dehalogenative deuteration of aryl halides in CH$_3$CN/D$_2$O, D$_2$O activation occurs to offer deuterium radicals (D$^•$) to promote the reaction. [13,32]

When H$_2$O was used, no deuterated alkane was detected regardless of the isotopic property of acetonitrile (Fig. 2Dc and Fig. 2Dd), confirming that D$_2$O is the solo deuteration source. In addition, it was observed that the Y_{C11-h} was higher than the combined yields of Y_{C11-d} and Y_{C11-h} obtained with D$_2$O (Fig. 2Da and 2Db). This result indicates an isotopic effect. Considering that the C$_{11}$-h obtained in the presence of D$_2$O (Fig. 2Da) is produced via reaction of alkyl radical with organic compound, the Y_{C11-h} in the absence of D$_2$O (Fig. 2Dd) should include C$_{11}$-h formed in the same way. Thus, the k_H/k_D value for C$_{11}$ production with H$_2$O or D$_2$O can be estimated to be 1.58. Similarly, the amount of C$_{22}$ obtained was higher, further supporting an isotopic effect with a k_H/k_D of 1.74. These findings suggest that the reaction rate is slower when breaking the D–OD bond in D$_2$O (Eq. 13 and 14) compared to the H–OH bond in H$_2$O, indicating that the activation of D$_2$O to form either radical species (Eq. 13 or 14) is the rate-determining steps (RDS) in this reaction system. However, the separate study revealed that the formation of $^•$OD radical (Eq. 14) would be minor due to the presence of LA. [62] Thus, the observed RDS would be the water reduction (Eq. 13). The plausible pathways for LA oxidation by the $^•$OD radical are likely minor (Eqs. 15 and 16).

Catalysis Science & Technology Accepted Manuscript

$$D_2O + e^- \rightarrow D^\bullet + OD^- \tag{13}$$

$$D_2O + h^+ \rightarrow {}^\bullet OD + D^+ \ \text{(minor)} \tag{14}$$

$$C_{11}H_{23}COOH + {}^\bullet OD \rightarrow {}^\bullet C_{11}H_{23} + CO_2 + HDO \ \text{(minor)} \tag{15}$$

$$C_{11}H_{23}COOH + {}^\bullet OD \rightarrow {}^\bullet C_{11}H_{22}COOH + HDO \ \text{(minor)} \tag{16}$$

As mentioned, the R_d did not reach 100% even under the optimized conditions. This suggests that another hydrogen (^1H) source contributing to the formation of C_{11}-h should still exist within the reaction system. Remaining possible hydrogen

sources are the organic molecules, such as LA and the produced undecane. It is proposed that the undecyl radical, photocatalytically generated from LA, could react with another LA (Eq. 17) or the produced alkanes (Eq. 18). The former will give deuterated or non-deuterated LA and the latter can give doubly deuterated undecane ($C_{11}H_{22}D_2$).

$${}^\bullet C_{11}H_{23} + C_{11}H_{23}COOH \rightarrow C_{11}H_{24} \ (C_{11}\text{-}h) + {}^\bullet C_{11}H_{22}COOH \tag{17}$$

$${}^\bullet C_{11}H_{23} + C_{11}H_{23}D \rightarrow C_{11}H_{24} \ (C_{11}\text{-}h) + {}^\bullet C_{11}H_{22}D \tag{18}$$
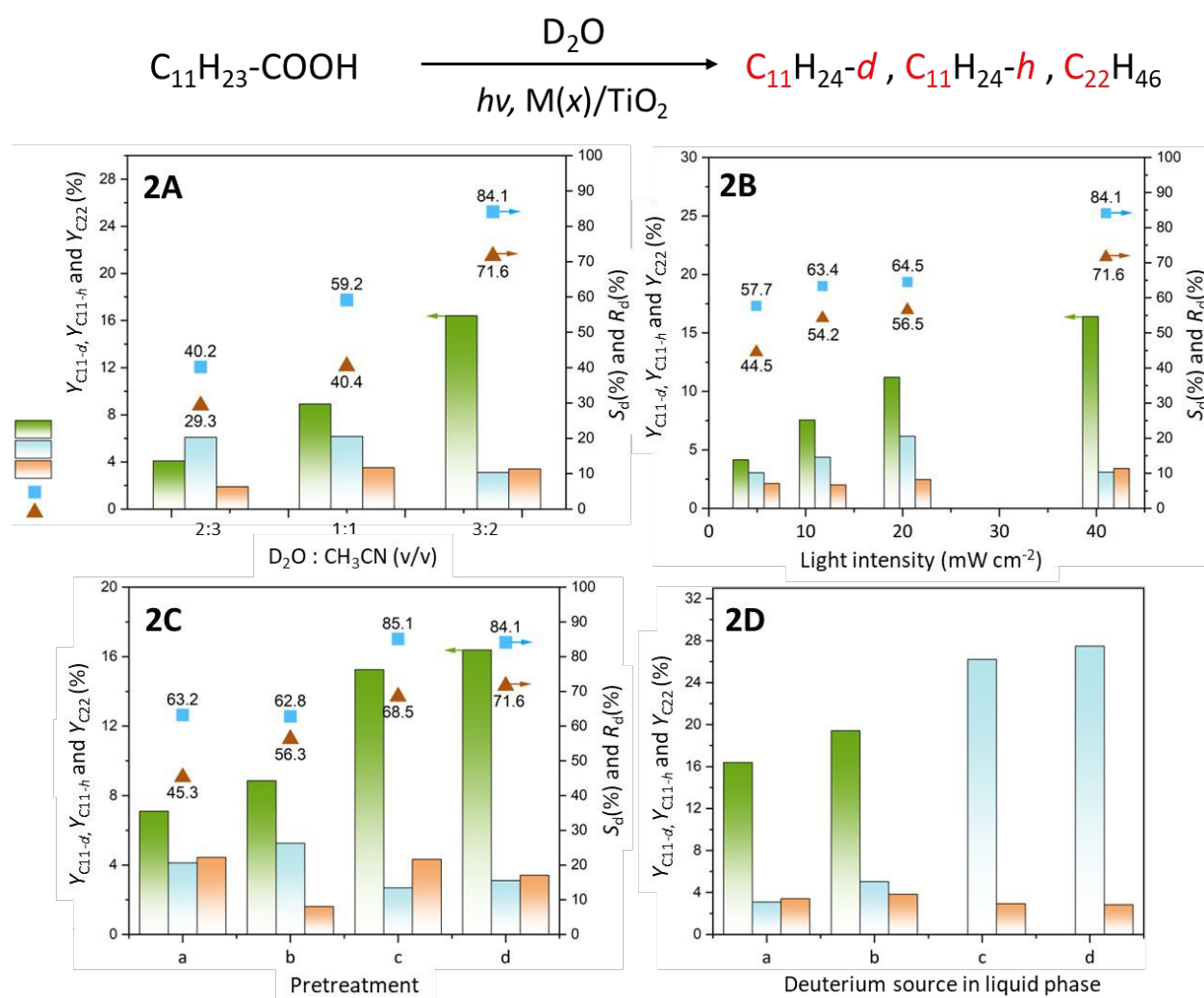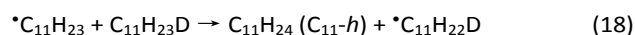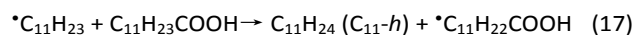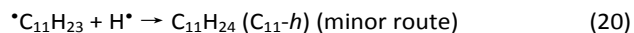

Fig. 2 Results of photocatalytic reaction tests with the Au(0.5)/TiO₂ sample. (A) Different ratios of CH₃CN and D₂O. (B) Dependence on light intensity. (C) Various pre-treatments, (a) without any pre-treatment, (b) with pre-irradiation in the presence of D₂O, (c) with pre-heating and pre-irradiation in the presence of D₂O, and (d) with pre-heating and pre-irradiation in the absence of D₂O as a standard condition. (D) Various liquid phases: (a) D₂O/CH₃CN, (b) D₂O/CD₃CN, (c) H₂O/CD₃CN, and (d) H₂O/CH₃CN. Other reaction conditions for panels A, B, C, and D are provided in the captions of Tables S5, S6, S7, and S8, respectively.

In addition, one may consider that protons (H⁺) formed from LA (Eq. 8) would be reduced by photoexcited electrons, potentially contributing to generation of C_{11}-h and thus decreasing the R_d. However, it cannot be ignored that the amount of LA (50 μmol) is limited whereas D₂O (56 mmol) is in

excess. However, it should be noted that the amount of LA (50 μmol) is limited, while D₂O (56 mmol) is present in large excess. The dissociated protons from LA react with the excess D₂O to form deuterated hydronium ions (D₂HO⁺), which can subsequently release D⁺ instead of H⁺, as shown in Eq. 19. This

suggests that protons (H^+) dissociated from LA are unlikely to be reduced by photoexcited electrons to generate $H\bullet$ radicals, and therefore contribute negligibly to the formation of C_{11}–h. Therefore, the pathway shown in Eq. 20 highly minor contributors to the overall product formation.

$$H^+ + D_2O \rightarrow HDO + D^+ \tag{19}$$

$$\bullet C_{11}H_{23} + H^\bullet \rightarrow C_{11}H_{24} (C_{11}\text{-}h) \text{ (minor route)} \tag{20}$$

Therefore, achieving complete selectivity to deuterated alkane would be difficult when using these kinds of organic acids like LA. To further increase the R_d value, the reaction rate of radical coupling between the alkyl radical and deuterium radical (Eq. 10) should be improved by further optimization of reaction conditions and improvement in photocatalyst properties.

Position of deuterium in the product. Considering that the photo-Kolbe reaction of acetic acid proceeds via decarboxylation to form methyl radical, one may expect that a linear carboxylic acid would generate a primary radical, which is an alkyl radical with the radical center at the terminal carbon originally bonded to the carboxy group. In the case of LA, this would initially form undecyl radical, with the radical center at the terminal carbon, $\bullet CH_2(CH_2)_9CH_3$. On the other hand, quantum chemical calculations using Gaussian 16 (Table S9) [63] showed that the secondary radical having the radical center at the second carbon from the terminal one, $CH_3\bullet CH(CH_2)_8CH_3$ is the most stable among the alkyl radicals.
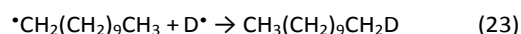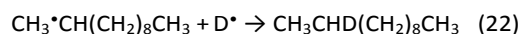
Radical intermediate species photocatalytically generated from LA were detected by using ESR measurement with a radical trapping method. A spin trapping reagent, DBNBS, trapped the radical species generated from LA with the Pt(0.1)/TiO$_2$ photocatalyst and formed some kinds of radical adducts. The spectrum is shown together with the calculated spectra in Fig. 3. Simulation of the obtained ESR spectra revealed that the spectrum consisted of two components: the major one (93.8 %) was an adduct trapping secondary radical, while the minor one (6.2 %) was the adduct trapping primary radical. In our previous work, [62] ESI-MS analysis clarified the presence of two major secondary radicals formed from LA: one of these radicals was secondary alkyl radical, represented as $CH_3(CH_2)_x\bullet CH(CH_2)_{8-x}CH_3$ (x=0–4), and another contained a carboxy group, represented as $CH_3(CH_2)_x\bullet CH(CH_2)_{9-x}COOH$ ($0 \leqslant x \leqslant 9$). These facts evidenced that the primary and the secondary alkyl radicals generated from LA were present in the presence conditions. When the radical species containing carboxy group reacts with deuterium radical ($D^\bullet$), it forms deuterated LA, meaning that it does not directly contribute to the formation of deuterated undecane in the initial stage. On the other hand, the primary and the secondary alkyl radicals can serve as the reaction intermediates, possibly forming corresponding deuterated undecane.

Among the possible secondary alkyl radicals, the one with the radical center at the second carbon from the terminal ($CH_3\bullet CH(CH_2)_8CH_3$) would be the most stable radical as mentioned above (Table S9). Since the primary radical initially generated from LA is thermodynamically unfavorable, radical

rearrangement reaction likely occurs. This rearrangement involves an intramolecular hydrogen atom transfer, which converts the primary radical into a more stable secondary radical with the radical center at the second carbon from the terminal (Eq. 21).

$\bullet CH_2(CH_2)_9CH_3$ (primary alkyl radical) $\rightarrow CH_3\bullet CH(CH_2)_8CH_3$ (secondary alkyl radical) (21)
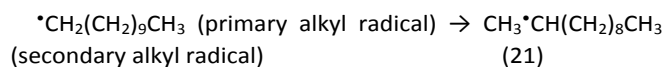
Therefore, the major deuterated undecane (C_{11}-d) obtained in the present system would be 2-deuterated n-undecane with deuterium incorporated at the second carbon from the terminal, $CH_3CHD(CH_2)_8CH_3$ (Eq. 22). This selectivity is determined thermodynamically. The 1-deuterated n-undecane would be the minor C_{11}-d product (Eq. 23)

$$CH_3\bullet CH(CH_2)_8CH_3 + D^\bullet \rightarrow CH_3CHD(CH_2)_8CH_3 \tag{22}$$

$$\bullet CH_2(CH_2)_9CH_3 + D^\bullet \rightarrow CH_3(CH_2)_9CH_2D \tag{23}$$

On the other hand, the main isomer of docosane (C_{22}) obtained was n-docosane, which should be formed via the radical-radical coupling of the primary undecyl radical (Scheme S2a). This could be explained by the difference in the reaction rate, including the migration rate. Two primary undecyl radicals initially produced via decarboxylation at the oxidation sites on the TiO$_2$ photocatalyst can immediately combine prior to the intramolecular hydrogen atom transfer (Eq. 21). On the other hand, the rate of crosscoupling between the undecyl radical and deuterium radical ($D^\bullet$) including the mass transfer rate would be relatively slow so that the intramolecular hydrogen atom transfer (Eq. 21) would occur before the crosscoupling of the radicals, producing $CH_3CHD(CH_2)_8CH_3$ (Eq. 22).

Proposed reaction mechanisms

Formation of deuterated undecane. Based on the results mentioned above, we propose a mechanism for the decarboxylation reaction of LA in the presence of D$_2$O leading to the formation of deuterated undecane (C_{11}-d_1) predominantly $CH_3CHD(CH_2)_8CH_3$ (Scheme 1). This mechanism is a one-photon radical process.

Upon photoirradiation, the TiO$_2$ photocatalyst generates electron-hole pairs. In the presence of a metal cocatalyst, the generated charge carries are spatially separated to some extent, with the electrons migrating to the cocatalyst and the holes reaching the TiO$_2$ surface. A molecule of LA ($C_{11}H_{23}COOH$) adsorbed on the TiO$_2$ surface is oxidized by a photogenerated hole, resulting in the formation of an unstable LA cation radical, $[C_{11}H_{23}COOH]^{+\bullet}$ (Scheme 1a). Alternative minor oxidation process is mediated by OD radical ($\bullet OD$) to form the LA cation radical (Scheme 1b). On the other hand, D$_2$O is reduced to deuterium radicals ($D^\bullet$) and OD$^-$ by photoexcited electrons on the metal cocatalyst (Eq. 15), which is suggested by the observation of isotope effect. This generation of hydroxy anions through reduction is balanced by the formation of protons via oxidation mentioned below.

The cation radical subsequently releases a proton (H^+), leading to the formation of either a carboxyl radical, $[C_{11}H_{23}COO]^\bullet$ (Scheme 1c) or an LA radical, $\bullet C_{11}H_{22}COOH$

(Scheme 1d). Among the two routes, the former directly generates a molecular CO_2 and an undecyl radical, $^\bullet C_{11}H_{23}$, where the initially produced primary undecyl radical, $^\bullet CH_2(CH_2)_9CH_3$, changes to the secondary radical, $CH_3{}^\bullet CH(CH_2)_8CH_3$ as a result of intramolecular hydrogen transfer prior to the final radical coupling step due to its higher thermodynamic stability as discussed above. Combining with deuterium radical, the target deuterated *n*-undecane featuring deuterium substitution at the second carbon from the terminal carbon, $CH_3CHD(CH_2)_8CH_3$ is formed (Scheme 1c). This is the major product C_{11}-*d* in this system. The latter, the LA radical, does not directly contribute to the undecane formation (Scheme 1d).

Three reaction pathways of alkyl radicals ($^\bullet C_{11}H_{23}$) are summarized in Scheme 1e-g. Only when the formed alkyl radical reacts with $^\bullet D$ (or D_2O), the deuterated alkane is formed (Scheme 1e). On the other hand, when it reacts with LA or alkyl radical, byproducts (C_{11}-*h* and C_{22}) are formed. To improve the R_d value, suppressing pathway f and increasing the pathway e are options worth considering. Furthermore, increasing the proportion of D_2O in the system or improving the hydrophilicity of the catalyst surface are both possible effective methods to enhance the R_d. Additionally, reducing the occurrence of pathway g is also beneficial for improving S_d.

(e) carboxy adduct (secondary)   (f) alkyl adduct (secondary)   (g) alkyl adduct (primary)
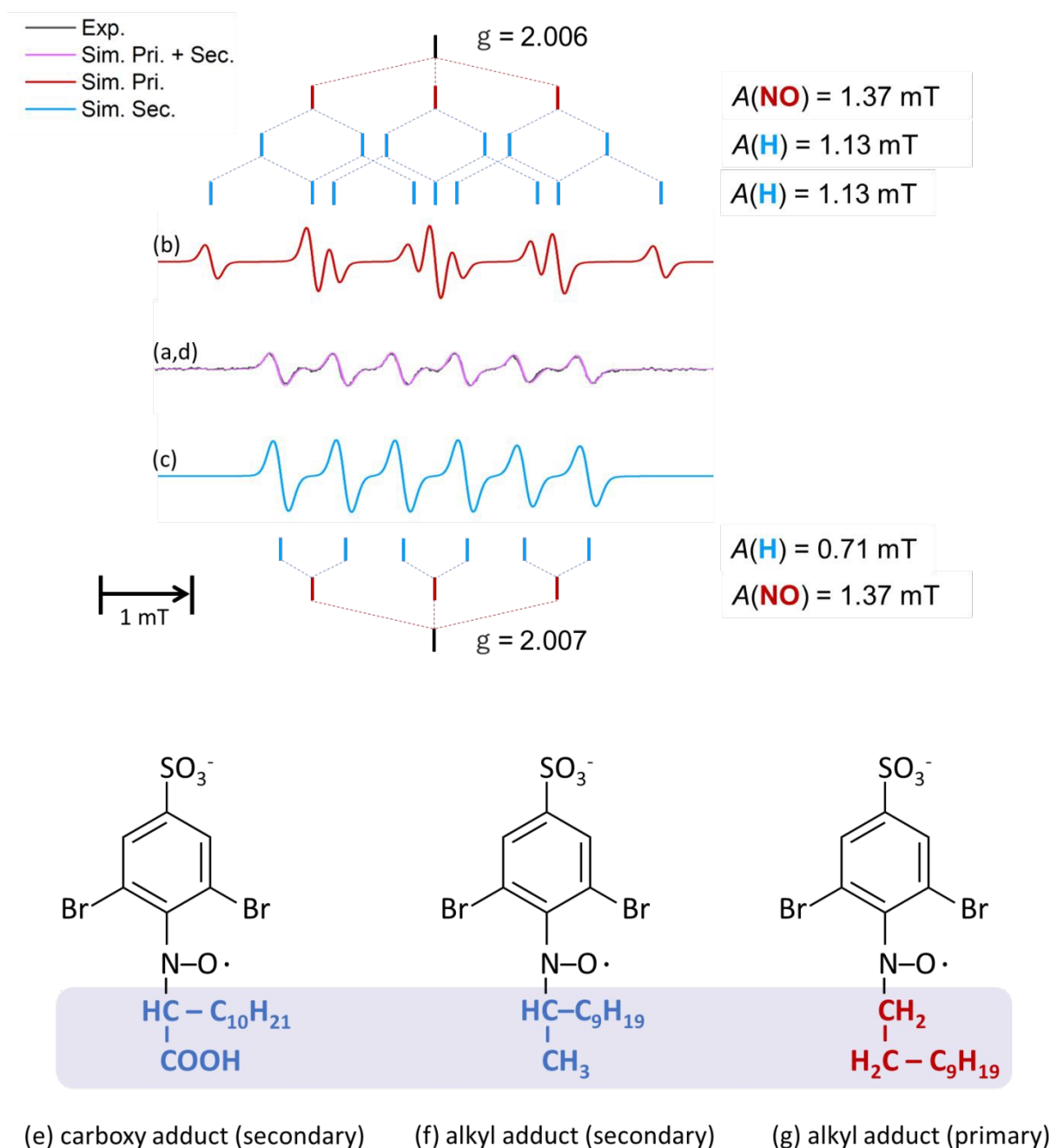
Fig. 3 Observed ESR spectrum of DBNBS-adduct-trapping radical species in supernatants of the resulting mixture after the photocatalytic reaction (a, black), and calculated spectra of primary radicals (b, red), secondary radicals (c, blue) and the sum of simulated spectra (d, overlapped to the observed spectrum), along with the representative spin adduct structures of carboxy secondary radical (e), alkyl secondary radical (f), and alkyl primary radical (g).The photocatalytic reaction was carried out in a mixed solvent of water (0.6 mL) and acetonitrile (0.4 mL), containing 10 mM of lauric acid ($C_{11}H_{23}COOH$), 10 mM of DBNBS, and 10 mg of the Pt(0.1)/TiO$_2$ photocatalyst. The simulation parameters for hyperfine coupling constants are A_{NO} = 1.37 mT, A_H = 1.13 mT for the primary radical; A_{NO} = 1.37 mT, A_H = 0.71 mT for the secondary radicals, respectively.

Side reactions. The main paragraph text follows directly on here. Here the side reactions are discussed. On the reduction sites, molecular hydrogen (H$_2$, HD, and D$_2$) might also be formed from homocoupling of two hydrogen radicals (H$^\bullet$ and D$^\bullet$) as shown in Eq. 5. The Pt cocatalyst is well known as a good catalyst for the hydrogen radical coupling compared to the Au cocatalyst, [64] which would be one of the reasons for the lower R_d value of the Pt/TiO$_2$ photocatalyst. The exact reason why the Au cocatalyst gave the higher R_d remains unclear. However, it is believed that its effectiveness lies in its ability to suppress such side reactions other than deuteration.

The undecyl radicals possibly react with some other chemical species, such as lauric acid, undecane, H$^\bullet$ radical, to form the undecane-h (Eqs. 21, 22, and 25) and with undecyl radical to give docosane (Scheme S2), which reduced the R_d value down to 85% even in the best conditions in the present study. Like we discussed in the previous section, because of the large amount of D$_2$O and small amount of LA, the H$^+$ or H radicals formed from LA are exposed to a large amount of heavy water and they are unlikely to be involved in the reaction. Therefore, the main reason for the incomplete selectivity, S_d and R_d are the reaction of the undecyl radical with other organic matters in the reaction system such as LA, undecane, and undecyl radical.

Additionally, when the alkyl carboxylic radical ($^\bullet C_{11}H_{22}COOH$) combines with a deuterium radical (D$^\bullet$) in route B, deuterated LA is formed. This may give doubly deuterated undecane ($C_{11}H_{22}D_2$), the presence of which was suggested by the GC-MS analysis (see Fig. S3). There are 2.42 μmol of C_{11}-d_2 after quantification. This result confirms that the formation of deuterated LA molecule ($C_{11}H_{22}DCOOH$), which provides further support for the supposed Scheme 1 (d). The formation of C_{11}-d is attributed to the reaction between alkyl radicals and LA molecule.

Light intensity. Based on the above mechanism, we propose an explanation for the increase in R_d with higher light intensity. First, the number of photogenerated electrons and holes increases as light intensity increases. On the oxidation side, the increase in holes promotes the formation of alkyl radicals, while on the reduction side, the increase in electrons enhances the production of D$^\bullet$ radicals as mentioned above. The reaction between the increased numbers of alkyl radicals and D$^\bullet$ radicals results in the formation of more deuterated alkanes in the system. In contrast, the reaction of alkyl radicals with LA produces non-deuterated alkane, but the amount of LA does not increase with light intensity. Consequently, high light

intensity preferentially leads to the production of deuterated alkane over non-deuterated alkane, thereby increasing the R_d.

Experimental

Catalyst preparation

All metal-loaded titanium oxide (M/TiO$_2$) photocatalysts were prepared by a photodeposition method with a commercial TiO$_2$ sample (Ishihara Sangyo Kaisha, ST-01, anatase, 300 m^{2}g^{-1}). Aqueous solutions of metal precursors, HAuCl$_4$ (Nacalai tesque, 99%), H$_2$PtCl$_6$ (Nacalai tesque, 99%), and PdCl$_2$ (Kishida Chemical, 99%), were used at concentrations of 9.89, 7.53, and 6.37 g L^{-1} as Au, Pt, and Pd, respectively.

The preparation of the Au(0.5)/TiO$_2$ sample is described as a representative example as follows. First, 2.0 g of TiO$_2$ powder was dispersed in 300 mL of ion-exchanged water and irradiated with a xenon lamp (PE300BUV, 300 W) for 30 min under magnetic stirring. Subsequently, 100 mL of methanol and 1 mL of the HAuCl$_4$ solution (9.894 g L^{-1} as Au) were added to the suspension. The mixture was stirred for 15 min without irradiation, followed by stirring for 1 h under light irradiation. After irradiation, the suspension was filtered and washed with over 500 mL of deionized water. The wet residue was dried in an electric oven at 353 K for 12 h, yielding a purple-colored powder of the Au(0.5)/TiO$_2$ sample. Here, x in M(x)/TiO$_2$ represents the metal loading amount as weight percent (wt%).

Other M(x)/TiO$_2$ photocatalysts were synthesized using similar procedures.
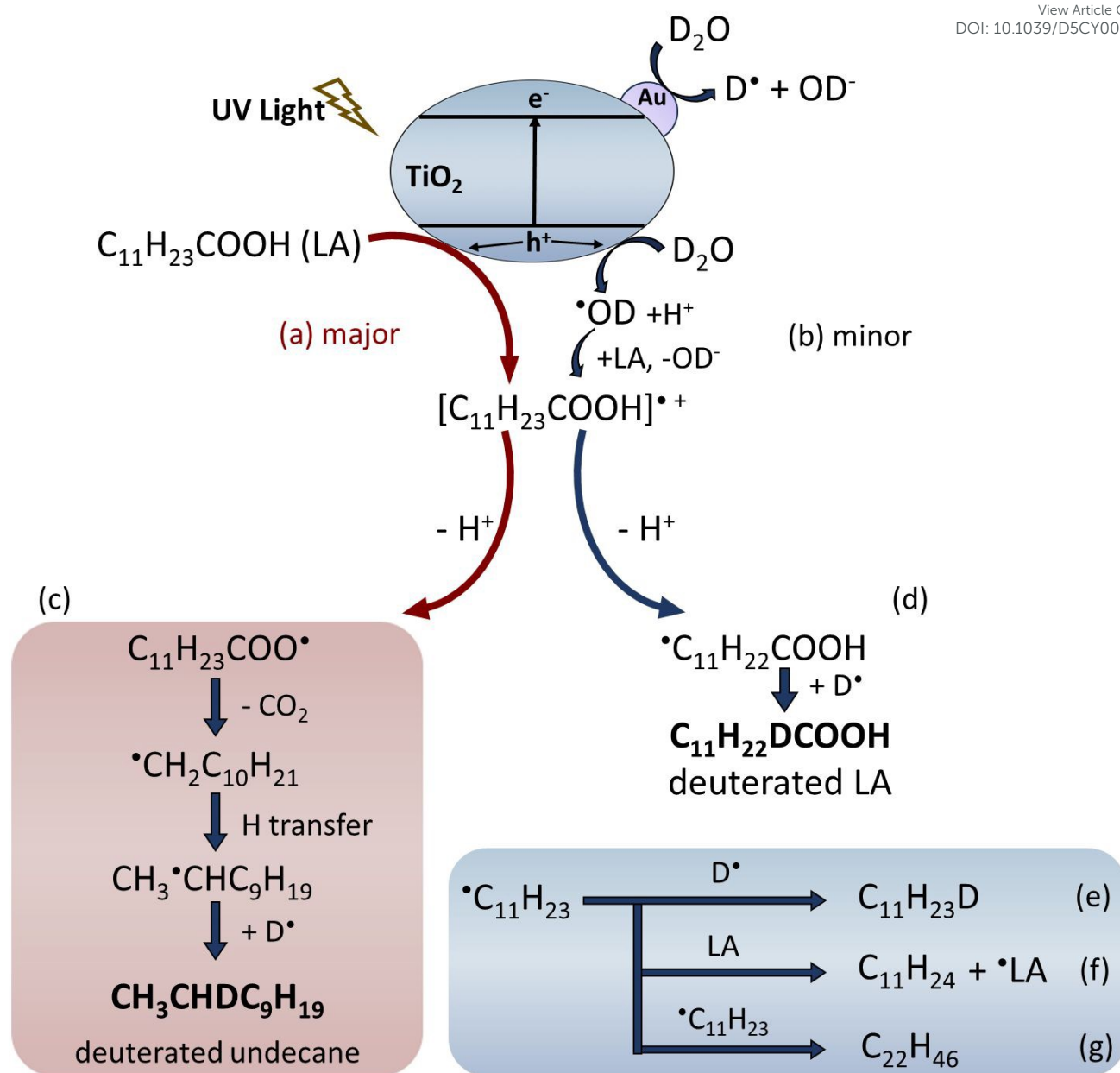
Synthesis of monodeuterated n-undecane with Grignard reagent

The n-[1-^{2}H$_1$]undecane (CH$_3$(CH$_2$)$_9$CH$_2$D) as a reference was synthesized by the Grignard reagent (see Supplementary Information, Scheme S1).

Photocatalytic reaction tests

The photocatalytic reaction test was conducted in a closed system using a capped 20 mL test tube. Typically, 50 mg of the

Scheme 1 Proposed mechanism for the production of deuterated undecane in the photocatalytically decarboxylation of LA in the presence of D_2O; formation of LA radical cation intermediates through (a) the direct hole oxidation or (b) indirect oxidation facilitated by $^\bullet OD$ radical, and successive alternative reactions of the LA radical cation for (c) the production of deuterated undecane and (d) the production of deuterated lauric acid, the latter of which does not directly produce deuterated undecane, and (e-g) three reaction pathways of alkyl radical.

photocatalyst was introduced and subjected to pre-heating at 450 K using a metal bath for 30 min in an argon gas flow (15 ml min⁻¹) to remove adsorbed water. Then the catalyst underwent pre-irradiation with a xenon lamp (PE300BUV, 300 W) for 15 min to clean the catalyst surface. Following the pre-heating and pre-irradiation, 5 mL of reactant solution containing LA (50 μmol), D_2O (3 mL), and acetonitrile (CH_3CN, 2 mL) was added to the test tube. The tube was sealed with a white silicone septum stopper and parafilm, the air was purged from the tube using an argon flow (15 ml min⁻¹) for 30

min, and the contents were stirred under light irradiation for the desired duration (typically, 180 min) using an optical filter that permitted light with wavelengths >360 nm to promote the photocatalytic reaction. The reaction is carried out at an ambient temperature of 25°C.

Optimization experiments were conducted under various conditions, including reaction time (Fig. 1), D_2O concentration, light intensity, pretreatment conditions, and deuterium source (Fig. 2).

ARTICLE

After the reaction, the liquid phase was filtered through a syringe equipped with a PTFE membrane filter and analyzed qualitatively and quantitatively using gas chromatography with GC-MS (Shimadzu QP-2020) and GC-FID (Shimadzu GC-2014), with n-decane ($C_{10}H_{22}$) as an internal standard. Details of the analysis for deuterated products and byproducts are described in the Supplementary information. The gas-phase products were detected by GC-TCD prior to the liquid-phase analysis.

The yield of product, Y_x (%) (x=C_{11}-d, C_{11}-h), Y_{C22} (%), the selectivity to deuterated undecane, S_d (%), and the ratio of deuterated undecane in the obtained undecane, R_d, were defined as follows (Eqs. 24–27):

$$Y_x \text{ (\%)} = 100 \times A_x / A_{\text{initial LA}} \quad (24)$$

$$Y_{C22} \text{ (\%)} = 100 \times 2 \times A_{C22} / A_{\text{initial LA}} \quad (25)$$

$$S_d \text{ (\%)} = 100 \times A_{C11\text{-}d} / (A_{C11\text{-}d} + A_{C11\text{-}h} + 2 \times A_{C22}) \quad (26)$$

$$R_d \text{ (\%)} = 100 \times A_{C11\text{-}d} / (A_{C11\text{-}d} + A_{C11\text{-}h}) \quad (27)$$

where A_x shows the amount of substance x. Specifically, $A_{\text{initial LA}}$ is the amount of initially introduced LA (50 μmol), $A_{C11\text{-}d}$ and $A_{C11\text{-}h}$ correspond to the amounts of [$^2H_1$]undecane ($C_{11}H_{23}D$, referred to as C_{11}-d) and undeuterated undecane ($C_{11}H_{24}$, referred to as C_{11}-h), respectively. GC-MS analysis also suggested the formation of a tiny amount of [$^2H_2$]undecane, referred to as C_{11}-d_2, which was included in $A_{C11\text{-}d}$. The amounts of docosane (n-docosane, $C_{22}H_{46}$, referred to as C_{22}) were referred to A_{C22}. Due to technical difficulties in the direct quantitative analysis of LA, total yield, Y_{total}(%) was used as an index of photocatalytic activity, which corresponds to the amount of the produced undecyl radical and defined as follows (Eq. 28).

$$Y_{\text{total}} \text{ (\%)} = 100 \times (A_{C11\text{-}d} + A_{C11\text{-}h} + 2 \times A_{C22}) / A_{\text{initial LA}} \quad (28)$$

Analyses of radical intermediates

Electron spin resonance (ESR) spectra of spin adducts were recorded at room temperature by a JES-RE1X spectrometer (JEOL Co. Ltd, Japan) equipped with a TE102 cavity using a quartz flat cell as described. [62] The Pt(0.1)/TiO$_2$ photocatalyst powder (10 mg) was put into a disposable test tube (D-10S, Nichiden-Rika Glass Co., Ltd., 75 mm height, o.d.=10 nm, i.d=8 mm) and pre-irradiated with a high-pressure Hg lamp (Ushio UI-501C) for 30 min to purify the catalyst surface. After the pre-irradiation, a reaction mixture of acetonitrile (CH$_3$CN, 0.4 mL), ultrapure water (H$_2$O, 0.6 mL), and LA (10 mM) were added to the test tube. Subsequently, 0.01 mM of DBNBS (3,5-dibromo-4-nitrosobenzenesulfonate sodium salt (C$_6$H$_2$NO$_4$SBr$_2$Na), Kyoto Spin Lab, ≥95%) was introduced as a spin-trapping reagent. The sample was then irradiated through an optical filter (wavelength ≥350 nm) for 10 min.

Following the photoirradiation, the mixture was centrifuged at 1.0×10^4 rpm for 5 min, and the supernatant was used for ESR measurement. Manganese (Mn^{2+}) dispersed in magnesium oxide (JEOL, Co. Ltd., Japan) served as the references for sensitivity and g-value calibration. The ESR spectra of DBNBS spin adducts were simulated using EasySpin 6.0.0 software on MATLAB®, employing the "garlic" core function without additional perturbations.

Conclusions

In this study, we successfully demonstrated a simple and sustainable method for the synthesis of deuterated alkanes using lauric acid ($C_{11}H_{23}$COOH) as an example. Metal-loaded TiO$_2$ photocatalysts facilitate photocatalytic decarboxylation of carboxylic acid, followed by successive deuteration using heavy water (D$_2$O), yielding deuterated alkane (deuterated undecane, $C_{11}H_{23}$D, C_{11}-d). Compared with the limited C_{11}-d yield and deuteration selectivity achieved with the bare TiO$_2$ sample, the Au(0.5)/TiO$_2$ photocatalyst sample showed a significantly improved performance, achieving a high yield ($Y_{C11\text{-}d}$=15.3%) and a deuterated undecane ratio in the obtained undecane (R_d=85.1%) in the present best conditions (Fig. 2Cc).

$C_{11}H_{23}$COOH molecule adsorbed on the TiO$_2$ surface is oxidized by a photogenerated hole, resulting in a LA cation radical, subsequently generates an undecyl radical, •$C_{11}H_{23}$. Combining with deuterium radical, the target deuterated n-undecane is formed.

The major product was identified as deuterated n-undecane with deuterium substitution predominantly occurring at the second carbon from the terminal carbon, CH$_3$CDH(CH$_2$)$_8$CH$_3$. Mechanistic investigations suggested that the limited selectivity arose from undesirable side reactions of the radical intermediate with other organic species, including the substrate, the derived radical species, and products. Further investigation to overcome these points is still desired.

These findings highlight a valuable strategy for synthesizing deuterated compounds by using heavy water (D$_2$O) as the deuterium source, providing a pathway for simple and highly selective deuteration reactions with broad potential applications.

Author contributions

Conflicts of interest

There are no conflicts to declare.

Data availability

The authors confirm that the data supporting the findings of this study are available within the manuscript and its ESI.† Raw data that support the findings of this study are available from the corresponding author, upon reasonable request.

Acknowledgements

References

1 H. Kragh, *Stud. Hist. Philos. Sci. B: Stud. Hist. Philos. Mod. Phys.*, 2012, **43**, 176–183.
2 C. S. Elmore, *Annu. Rep. Med. Chem.*, 2009, **44**. 515–534.
3 Y. Y. Loh, K. Nagao, A. J. Hoover, D. Hesk, N. R. Rivera, S. L. Colletti, I. W. Davies and D. W. C. Macmillan, *Science*, 2017, **358**, 1182–1187.
4 W. Ou, C. Qiu and C. Su, *Chin. J. Catal.*, 2022, **43**, 956–970.
5 S. H. DeWitt and B. E. Maryanoff, *Biochemistry*, 2018, **57**, 472–473.
6 C. Scnmidt, *Nat. Biotechnol.*, 2017, **35**, 493–495.
7 S. Kopf, F. Bourriquen, W. Li, H. Neumann, K. Junge and M. Beller, *Chem. Rev.,* 2022, **122**, 6634–6718
8 H. Li, M. Shabbir, W. Li and A. Lei, *Chin. J. Chem.*, 2024, **42**, 1145–1156.
9 G. Prakash, N. Paul, G. A. Oliver, D. B. Werz and D. Maiti, *Chem. Soc. Rev.,* 2022, **51**, 3123–3163.
10 N. Li, Y. Li, X. Wu, C. Zhu and J. Xie, *Chem. Soc. Rev.,* 2022, **51**, 6291–6306.
11 P. L. Norcott, *Chem. Commun.,* 2022, **58**, 2944–2953.
12 R. Zhou, L. Ma, X. Yang and J. Cao, *Org. Chem. Front.,* 2021, **8**, 426–444.
13 Y. Dong, Y. Su, L. Du, R. Wang, L. Zhang, D. Zhao and W. Xie, *ACS Nano*, 2019, **13**, 10754–10760.
14 A. Di Giuseppe, R. Castarlenas and L. A. Oro, *C. R. Chim.*, 2015, **18**, 713–741.
15 W. J. Kerr, D. M. Lindsay, P. K. Owens, M. Reid, T. Tuttle and S. Campos, *ACS Catal.*, 2017, **7**, 7182–7186.
16 P. Ranjan, S. Pillitteri, E. V. Van Der Eycken and U. K. Sharma, *Green Chem.,* 2020, 22, 7725–7736
17 J. Atzrodt, V. Derdau, T. Fey and J. Zimmermann, *Angew. Chem. Int. Ed.*, 2007, 46, 7744–7765.
18 Y. Chang, A. Yesilcimen, M. Cao, Y. Zhang, B. Zhang, J. Z. Chan and M. Wasa, *J. Am. Chem. Soc.*, 2019, **141**, 14570–14575.
19 A. Martins and M. Lautens, *Org. Lett.*, 2008, **10**, 4351–4353.
20 F. Bourriquen, N. Rockstroh, S. Bartling, K. Junge and M. Beller, *Angew. Chem. Int. Ed.*, 2022, **61**, e202202423.
21 T. Kurita, K. Hattori, S. Seki, T. Mizumoto, F. Aoki, Y. Yamada, K. Ikawa, T. Maegawa, Y. Monguchi and H. Sajiki, *Chem. Eur. J.,* 2008, **14**, 664–673.
22 W. N. Palmer and P. J. Chirik, *ACS Catal.*, 2017, **7**, 5674–5678.
23 V. Pfeifer, T. Zeltner, C. Fackler, A. Kraemer, J. Thoma, A. Zeller and R. Kiesling, *Angew. Chem. Int. Ed.*, 2021, **60**, 26671–26676.
24 Z. Yu, W. Wang and L. Chen, *J. Labelled Comp. Radiopharm*, 2011, **54**, 352–356.
25 C. Zhang, Z. Shen, L. Tian and L. Chen, *J. Labelled Comp. Radiopharm.*, 2012, **55**, 401–405.
26 M. Fang and K. R. Cadwallader, *J. Agric. Food Chem.*, 2013, **61**, 3580–3588.
27 G. Srinivas, V. K. P. Unny, K. Mukkanti and B. M. Choudary, *J. Labelled Comp. Radiopharm.*, 2013, **56**, 325–329.
28 J. Atzrodt, V. Derdau, W. J. Kerr and M. Reid, *Angew. Chem. Int. Ed.*, 2018, **57**, 3022–3047.
29 J. Martin, J. Eyselein, S. Grams and S. Harder, *ACS Catal.*, 2020, **10**, 7792–7799.
30 C. S. Donald, T. A. Moss, G. M. Noonan, B. Roberts and E. C. Durham, *Tetrahedron Lett.*, 2014, **55**, 3305–3307.
31 M. Kuriyama, N. Hamaguchi, G. Yano, K. Tsukuda, K. Sato and O. Onomura, *J. Org. Chem.*, 2016, **81**, 8934–8946.
32 C. Liu, Z. Chen, C. Su, X. Zhao, Q. Gao, G. H. Ning, H. Zhu, W. Tang, K. Leng, W. Fu, B. Tian, X. Peng, J. Li, Q. H. Xu, W. Zhou and K. P. Loh, *Nat. Commun.*, 2018, **9**, 80.
33 T. Luo, Z. Wang, Y. Chen, H. Li, M. Peng, F. Tuna, E. J. L. McInnes, S. J. Day, J. An, M. Schröder and S. Yang, *Angew. Chem. Int. Ed.*, 2023, **62**, e202306267.
34 C. S. Turchi and D. F. Ollis, *J. Catal.* 1990, **122,** 178–192.
35 T. Yang, J. Peng, Y. Zheng, X. He, Y. Hou, L. Wu and X. Fu, *Appl Catal B*, 2018, **221**, 223–234.
36 L. B. Reuterglrdh and M. Langphasuk, *Chemosphere*, 1997, **35**, 585–596.
37 Y. Sari, P. L. Gareso, B. Armynah, D. Tahir, *Int. J. Hydrog. Energy*, 2024, **55**, 984–996.
38 A. Fujishima, T. N. Rao and D. A. Tryk, *J. Photochem. Photobiol. C*, 2000, **1**, 1–21.
39 M. Ni, M. K. H. Leung, D. Y. C. Leung and K. Sumathy, *Renew. Sustain. Energy Rev.*, 2007, **11**, 401–425.
40 J. C. Smart, B. L. Pinsky, M. F. Fredrich and V. W. Day, *J. Am. Chem. Soc.*, 1979, **101**, 4373–4374.
41 K. Yamaguti and S. Sato, *J. Chem. Soc., Faraday Trans. 1*, 1985, **81**, 1237–1246.
42 T. Kawai and T. Sakata, *Chem. Phys. Lett.*, 1980, **72**, 87–89.
43 S. Sato and J. M. White, *Chem. Phys. Lett.*, 1980, **72**, 83–86.
44 H. Eidsvåg, S. Bentouba, P. Vajeeston, et al., *Molecules*, 2021, **26**, 1687.
45 H. Abdullah, M. M. R. Khan, H. R. Ong and Z. Yaakob, *J. CO₂ Util.*, 2017, **22**, 15–32.
46 A. Hammad, A. Anzai, X. Zhu, A. Yamamoto, A. Ootsuki, T. Yoshida, A. EL-Shazly, M. Elkady and H. Yoshida, *Catal. Letters*, 2020, **150**, 1081–1088.
47 H. Yuzawa and H. Yoshida, *Chem. Lett.*, 2013, **42**, 1336–1343.
48 D. Friedmann, A. Hakki, H. Kim, W. Choi and D. Bahnemann, *Green Chem.*, 2016, **18**, 5391–5411.
49 S. Kohtani, E. Yoshioka, K. Saito, A. Kudo and H. Miyabe, *Catal. Commun*, 2010, **11**, 1049–1053.
50 K. Imamura, T. Yoshikawa, K. Hashimoto and H. Kominami, *Appl. Catal. B*, 2013, **134–135**, 193–197.
51 N. Hoffmann, *Aust. J. Chem.*, 2015, **68**, 1621–639.
52 B. Kraeutler and A. J. Bard, *J. Am. Chem. Soc.*, 1978, **100**, 2239–2240.
53 B. Kraeutler and A. J. Bard, *J. Am. Chem. Soc.*, 1978, **100**, 5985–5992.
54 K. Zou, A. Yamamoto and H. Yoshida, *Catal. Today*, 2024, **425**, 114354.
55 N. Li, Y. Ning, X. Wu, J. Xie, W. Li and C. Zhu, *Chem Sci.*, 2021, **12**, 5505–5510.
56 Y. He, H. Yang, D. Gao, J. Ma, Y. Shao, G. An and G. Li, *Chin. J. Org. Chem.*, 2021, **41**, 4725–4731.

ARTICLE

57 Z. Huang, Z. Zhao, C. Zhang, J. Lu, H. Liu, N. Luo, J. Zhang and F. Wang, *Nat. Catal.*, 2020, **3**, 170–178.

58 H. Yoshida, *Adv. Energy Sustain. Res.*, 2025, 2400439.

59 S. Park, J. Jeong, K. I. Fujita, A. Yamamoto and H. Yoshida, *J. Am. Chem. Soc.*, 2020, **142**, 12708–12714.

60 H. Yuzawa, M. Aoki, K. Otake, T. Hattori, H. Itoh and H. Yoshida. *J. Phys. Chem*. C., 2012, **116**, 25376–25387.

61 H. Yuzawa, J. Kumagai and H. Yoshida. *J. Phys. Chem. C.*, 2013, **117**, 11047–11058.

62 G. Lee, R. Maruyama, K. Zou, H. Huang, K. Oyama, H. Yoshida and J. Kumagai, *J. Phys. Chem. C.*, 2025, **129**, 402–414.

63 M. J. Frisch, G. W. Trucks, H. B. Schlegel, G. E. Scuseria, M. A. Robb, J. R. Cheeseman, G. Scalmani, V. Barone, G. A. Petersson, H. Nakatsuji, et al., Gaussian 16, 2019, Wallingford CT: Gaussian, Inc.; Vers. Revision C.02.

64 K. Zou, A. Yamamoto and H. Yoshida, *Int. J. Hydrogen Energy.*, 2024, **91**, 989–996.

Catalysis Science & Technology Accepted Manuscript

Data availability

The authors confirm that the data supporting the findings of this study are available within the manuscript and its ESI. † Raw data that support the findings of this study are available from the corresponding author, upon reasonable request.